Available online at www.sciencedirect.com
ScienceDirect
Journal of the European Ceramic Society 31 (2011) 1865–1871
www.elsevier.com/locate/jeurceramsoc

Nanoscale elastic–plastic deformation and stress distributions of the C plane of sapphire single crystal during nanoindentation

W.G. Mao [a,b], Y.G. Shen [a,*], C. Lu [c]

[a] Department of Manufacturing Engineering and Engineering Management (MEEM), City University of Hong Kong, Kowloon, Hong Kong
[b] Key Laboratory of Low Dimensional Materials and Application Technology, Ministry of Education, Xiangtan University, Hunan 411105, China
[c] Department of Mechanical Engineering, Curtin University, Perth, WA 6845, Australia

Received 31 August 2010; received in revised form 27 January 2011; accepted 7 April 2011
Available online 4 May 2011

Abstract

The nanoscale elastic–plastic characteristics of the C plane of sapphire single crystal were studied by ultra-low nanoindentation loads with a Berkovich indenter within the indentation depth less than 60 nm. The smaller the loading rate is, the greater the corresponding critical pop-in loads and the width of pop-in extension become. It is shown that hardness obviously exhibits the indentation size effect (ISE), which is 46.7 ± 15 GPa at the ISE region and is equal to 27.5 ± 2 GPa at the non-ISE region. The indentation modulus of the C plane decreases with increasing the indentation depth and equals 420.6 ± 20 GPa at the steady-state when the indentation depth exceeds 60 nm. Based on the Schmidt law, Hertzian contact theory and crystallography, the possibilities of activation of primary slip systems indented on the C surface and the distributions of critical resolved shear stresses on the slip plane were analyzed.

Keywords: Single crystal sapphire; Nanoindentation; Critical resolved shear stress; Multiple pop-in events; Mechanical properties

1. Introduction

Sapphire (α-Al_2O_3) is an important crystal material due to its high hardness, chemical inertness, superior mechanical performance, and thermodynamic stability.[1–3] Generally, sapphire is brittle and its brittle-to-ductile transition temperature is ~1373 K. However, the plastic deformation of sapphire crystals may occur under low loads at room temperature.[4] Recently, the evaluation of the initial stages of plasticity and elastic–plastic deformation properties of sapphire with different surface orientations at room temperature have been extensively investigated by nanoindentation tests.[4–12] These studies show that single and/or multiple displacement discontinuity (pop-in) events during loading are found to distinguish between the fully elastic and the elastic-plastic regimes, associated with the nucleation of dislocations. As we know, the C plane (0 0 0 1) of sapphire is generally selected as a calibration medium during nanoindentation[13] and substrate in the preparation of many kinds of functional thin film/substrate systems.[14,15] It is necessary to study the mechanical properties of the C plane under different size scales and measurement conditions. Although many studies have been done on elastic-plastic behaviors of the C plane by micro-/nano-indentation with relatively large Berkovich or spherical indenters, the interpretation of indentation results obtained at room temperature is not straightforward because these indentation measurements are strongly affected by factors such as the anisotropic elasticity of sapphire, surface roughness, the radius and shape of indenter tip, loading rate and indentation depth.[4–8] In this paper, the nanoscale elastic/plastic deformation and mechanical properties of the C plane have been systematically studied by depth-sensing nanoindentation experiments at room temperature. The contact area function and radius of the Berkovich tip were carefully calibrated under very small indentation depth by nanoindentation and atomic force microscopy (AFM) instruments. The mechanical properties and surface deformation mechanism of sapphire crystal indented on the C plane were analyzed under the anisotropic elastic characteristic and small indentation depth. The critical resolved shear stresses (CRSS) at slip planes were evaluated with the aid of the Hertzian contact theory, compared with the corresponding the-

* Corresponding author. Tel.: +852 2784 4658; fax: +852 2788 8423.
E-mail address: meshen@cityu.edu.hk (Y.G. Shen).

0955-2219/$ – see front matter © 2011 Elsevier Ltd. All rights reserved.
doi:10.1016/j.jeurceramsoc.2011.04.012

oretical shear strength. The experimental and analytical results would greatly shed light on the understanding of the nanoscale deformation features of sapphire crystal indented on the C plane.

2. Experimental

The samples of sapphire crystal were obtained from Semiconductor Wafer, Inc in Taiwan. As specified by the manufacturer, these single crystals were *C*-axis oriented, double-side polished, and free from defects and residual stress with a root-mean-square roughness < 0.2 nm. Our X-ray diffraction θ–2θ measurements confirmed that the samples were high quality single crystals. All nanoindentation experiments were conducted using an indenter (Triboscope, Hysitron Inc.) equipped with a three-sided pyramidal Berkovich diamond tip and an in situ scanning probe microscopy (SPM) at room temperature. The force and displacement sensitivities of the instrument are 100 nN and 0.2 nm, respectively. Indentations were performed under a variety of peak loads in the range of 0.7–8 mN. For all nanoindentation tests, the loading and unloading times were 20 s and holding time was set as 10 s at the peak indent loads, which resulted in a series of different loading rates ranging from 0.035 to 0.4 mN/s. To obtain reliable data, each cycle was repeated 8 times. The thermal drift was kept below ± 0.05 nm/s for all indentations.

3. Results and discussion

3.1. Calibration of indenter tip radius

Prior to nanoindentation tests, the contact area function and effective indenter tip radius should be carefully calibrated by using a standard sample such as fused quartz.[16] As shown in Fig. 1, the experimental data are fitted by the area function[16]

$$A = C_0h_c^2 + C_1h_c + C_2h_c^{1/2} + C_3h_c^{1/4} + \cdots + C_8h_c^{1/128} \quad (1)$$

where C_O, C_1, …, C_8 are constants, and h_c is the contact depth. The lead term describes a perfect Berkovich indenter; others represent deviations from the Berkovich geometry due to blunting at the tip. These coefficients should be fitted by the A and h_c data based on the relevant indentation depth range.[16] In this work, we focus on the two different ranges of 10–100 nm and 100–500 nm indentation depths. Under the small range of 10–100 nm, the Berkovich tip is generally regarded as spherical or parabola revolution.[13,16,17] The relationship between A and h_c can be well described by a simple two-parameter relationship, $A = C_0h_c^2 + C_1h_c$. In the limit of $h_c \ll R$ (here R is the radius of indenter tip), the relationship can approximately reduce to $A = 2\pi Rh_c$.[17,18] As shown in Fig. 1, for $h_c < 60$ nm, the relationship was found to be $A = 25.8h_c^2 + 752.7h_c$ for our Berkovich indenter, where the units of A and h_c are nm^2 and nm, respectively. Consequently, the tip radius R obtained from the second term, $C_1 = 2\pi R$, is equal to 120 ± 5 nm. However, for a relative large indentation range of 100–500 nm, we must re-calibrate the tip area function,[16] $A = 24.5h_c^2 + 780.2h_c + 417h_c^{1/2}$. Therefore, according to the indentation depth of sapphire single crystal, two different tip area functions are chosen to analyze the indentation data.

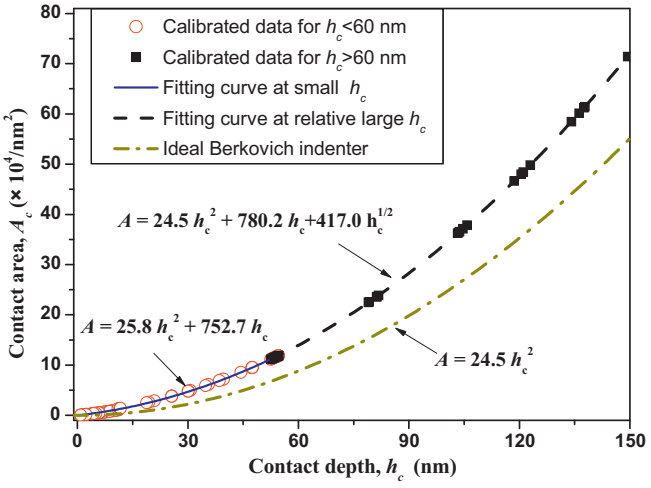

Fig. 1. The calibrated function of indenter contact area and contact depth with standard fused quartz sample.

To verify the tip radius, the three-dimensional geometry of an instrumented indenter was carefully measured by atomic force microscopy (AFM). The AFM image data can be obtained by scanning the Berkovich tip apex. For each AFM image, scanning is along the orthogonal directions of cross-sections through the apex of indenter, which are parallel to the x- and y-directions, respectively, as shown in Fig. 2(a). A parabolic curve was fitted to the near-apex region of the cross-sectional data, as shown in Fig. 2(b) and R was determined from the parabolic equation at the apex location. To discern the difference,[19] four curves are dissociated by adjusting the values of relative vertical distance in Fig. 2(b). It is shown that the average value of the tip radius, $R = 130 \pm 10$ nm obtained by AFM, is slightly larger than that from nanoindentation measurements. In the subsequent analysis, R is regarded as about 125 nm.

3.2. Characteristics of load–displacement curves

Fig. 3 shows the total of the 8 representative load–displacement (P–h) curves of the indented C plane during nanoindentation. It is obvious that multiple displacement discontinuities or pop-in events occur during loading. The load corresponding to the first pop-in event is defined as the critical indentation load P_{cr}, which varies in the range of 0.40–0.62 mN (see inset in Fig. 3). The width of pop-in extension is denoted with Δh_{cr} due to the slip of activated dislocation. The pop-in phenomena are consistent with the earliest observations reported by Page[4,5,7] However, P_{cr} in their studies were much higher than P_{cr} in our work, which may ascribe to the radius magnitude of indenter tip. It is also found the fluctuation phenomena of the P_{cr} among these pop-in events, which is similar to other experimental results.[20,21] The reason may be due to the effects of thermal drift and surface roughness under the condition of ultra-low loads.

In nanoindentation tests, the loading rate $\dot{P}$ ranges from 0.035–0.4 mN/s. The relationships of the average P_{cr}, average pop-in extension width Δh_{cr} and $\dot{P}$ for the C plane are shown

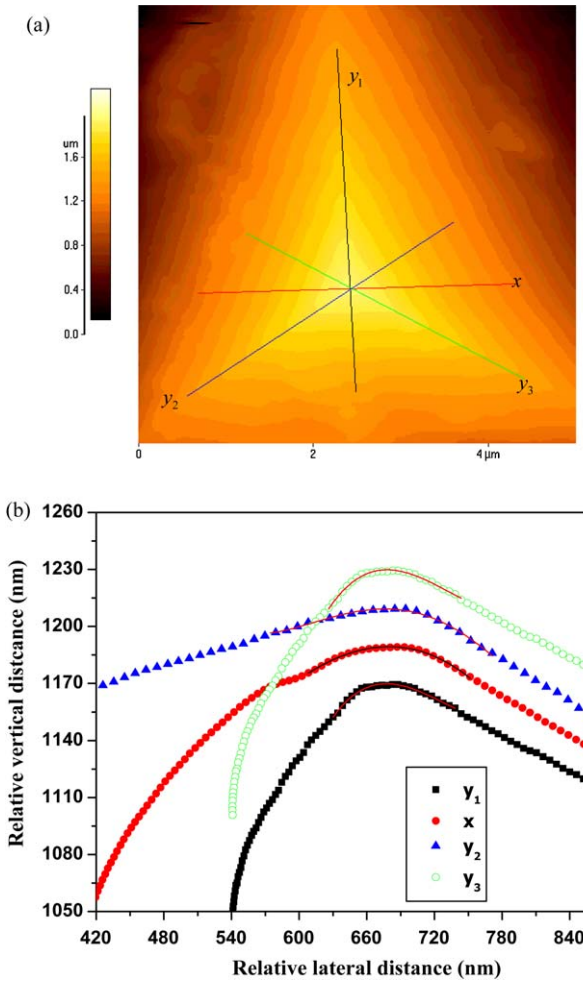

Fig. 2. (a) AFM observations of 3D surface morphology of a Berkovich indentation probe and (b) data analysis of tip radius variations along x, y_1, y_2 and y_3 cross-sections and the parabolic fitting curves near the apex, which are utilized to estimate the tip radius.

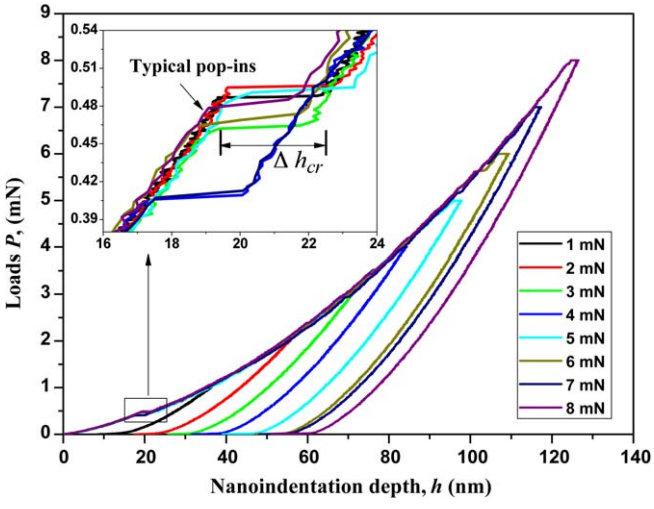

Fig. 3. Typical load–displacement curves of sapphire crystal indented on the C plane under ultra-low nanoindentation loads at room temperature. Inset is the magnified region indicated by a rectangle, which presents the first pop-in during loading.

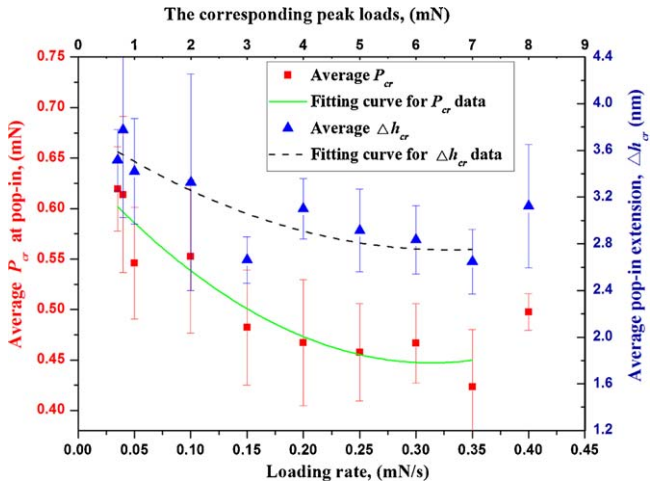

Fig. 4. The relationship of loading rates, critical pop-in loads and pop-in extension width under the different peak loadings.

in Fig. 4. It is seen that P_{cr} and Δh_{cr} decrease gradually with increasing $\dot{P}$ with the range from 0.035 to 0.35 mN/s. It is more obvious under the lower loading rate and smaller indentation depth of $h < 60$ nm. When $\dot{P}$ is small, the slip plane of the primary slip system in sapphire crystal has enough time to be stressed and activated, which results in the large width of pop-in extension Δh_{cr}, i.e., the burst displacement. If $\dot{P}$ rapidly increases, however, the elastic and elastic–plastic transitions of sapphire crystal are too fast to adequately slip or twinning. Thus, P_{cr} and Δh_{cr} may decrease, and even the pop-in phenomena may disappear. Under the large $\dot{P}$, Tymiak et al. found that the influence of loading rate was not clear for the C plane during nanoindentation with a 100 nm cube corner indenter tip.[4] Therefore, the loading rate and indentation depth range have an important influence on the elastic–plastic deformation of sapphire crystal, especially at nanoscales.

In this paper, we would emphasize on the first pop-in phenomenon of the C plane corresponded to the initial elastic-plastic transition of sapphire crystal. After indentation, to clarify the surface morphology of residual impression indented by the Berkovich indenter with a peak load of 1 mN, the in situ SPM observations of nanoindentation instrument are performed, as shown in Fig. 5, which may provide additional insight into the mechanisms of indentation-induced deformation. It is not observed from Figs. 5(a) and (b) apparent linear surface feature and cracking near the vicinity of the impression surface after the elastic-plastic transition of the C plane. The results are similar to the previous observations obtained by conical indenter.[4] The different linear topography profiles across the center of the impression are shown in Fig. 5(c). It is demonstrated that, even for hard and brittle sapphire, there are slight pile-ups with the relative high amplitude (see Fig. 5(c)). The maximum height of pile-ups is about 1.5 nm. The maximum indentation depth determined from these profiles is about 9.4 nm, which is close to the residual impression depth (10.2 nm) recorded by the corresponding load–displacement curve of 1 mN peak load in Fig. 3. The subtle discrepancy may be due to the finite curvature radius of the scanning probe tip and elastic recovery

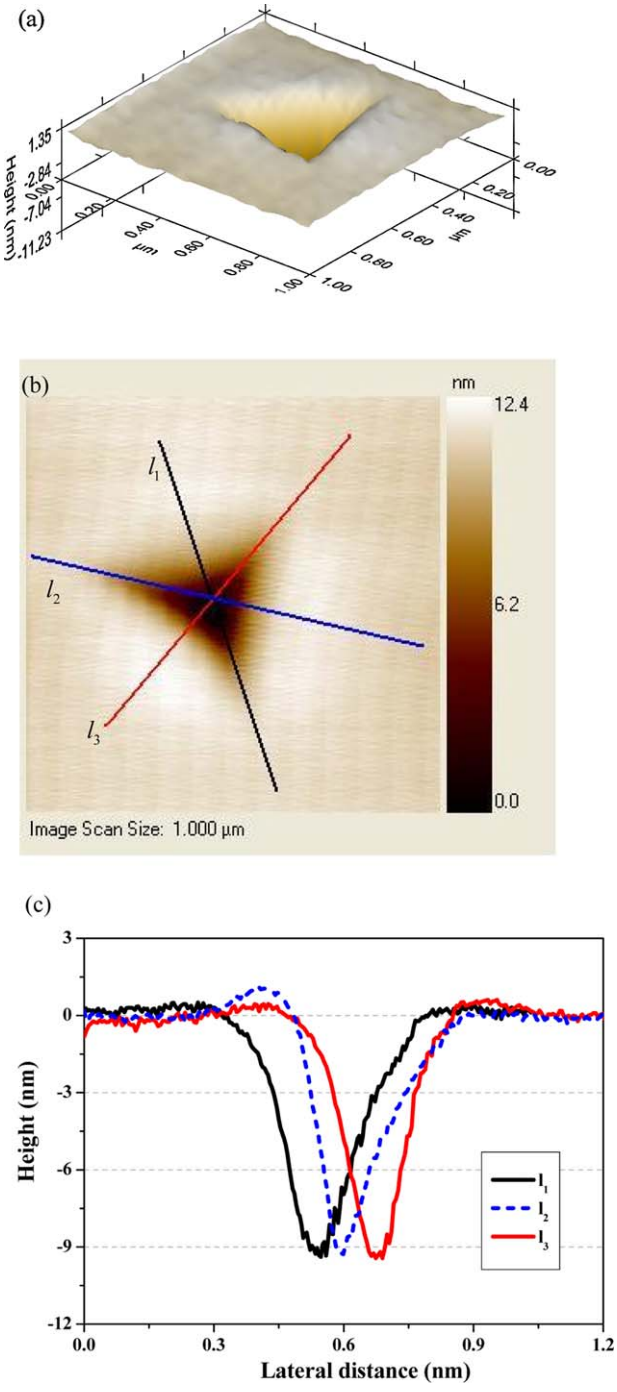

Fig. 5. Three-dimensional (a), top view (b) and cross-sectional (c) of SPM observations obtained from the indentation impression in a contact mode, where the peak indentation load is only 1 mN.

in unloading, which prevents it from reaching the impression bottom.

3.3. Hardness and indentation modulus

Based on the Oliver–Pharr method,[18] the hardness H of the C plane and the effective indentation modulus E_r of the indentation system can be directly obtained from nanoindentation instrument. It is found that H displays strong indent

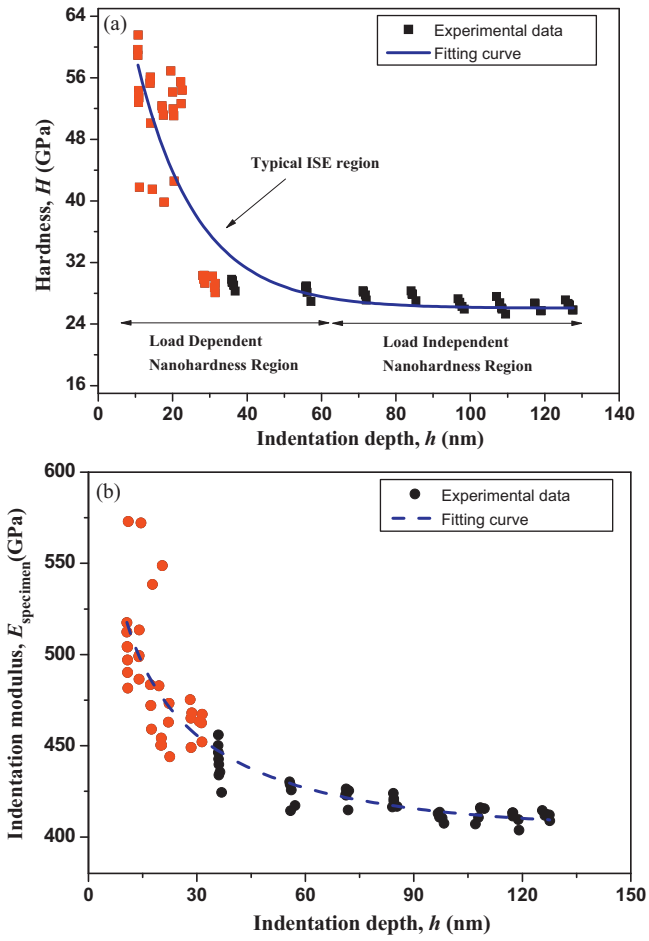

Fig. 6. Effect of indentation depth on hardness and indentation modulus of the C plane under different loading rates and peak loads.

size effect (ISE) within the range of $h < 60$ nm, i.e., the value decreases with the increase of indentation depth, as shown in Fig. 6(a). At the ISE region, the average H is 46.7 ± 15 GPa, as shown with the red square. At the load-independent hardness region, the range of H equals 27.5 ± 2 GPa, which is in good agreement with the result of 28.9 ± 2.3 GPa.[22] The indentation modulus $E_{specimen}$ of the C plane can be determined by contact mechanics.[23] Here, $1/E_r = 1/E_{specimen} + (1 - \nu_i^2)/E_i$, where $E_i = 1141$ GPa and $\nu_i = 0.07$ are Young's modulus and Poisson's ratio of the Berkovich diamond indenter.[13,18,24] It is seen in Fig. 6(b) that the values of $E_{specimen}$ are closely related to the indentation depth. Similar experimental phenomena have also been reported in previous studies.[25,26] When h is less than 60 nm, $E_{specimen}$ decreases with the increase of h and is equal to 493.2 ± 50 GPa, as indicated by the red dots in Fig. 6(b). If h exceeds to 60 nm, $E_{specimen}$ gradually goes into saturation and is equal to 420.6 ± 20 GPa. For sapphire with the trigonal symmetry, there are six independent elastic constants. These elastic constants were determined as $C_{11} = 496.72$, $C_{12} = 163.4$, $C_{13} = 110.73$, $C_{33} = 497.98$, $C_{14} = -23.49$ and $C_{44} = 148$ GPa.[13] The Poisson's ratio, shear modulus G and Young's modulus $E_{(0001)}$ along the C-axis relevant to indentation is given, respectively, by $\upsilon = C_{13}/(C_{11} + C_{12})$, $G = (C_{11} - C_{12})/2$ and $E_{(0001)} = C_{33} - 2\upsilon C_{13}$ under purely elastic deformation.[27] So,

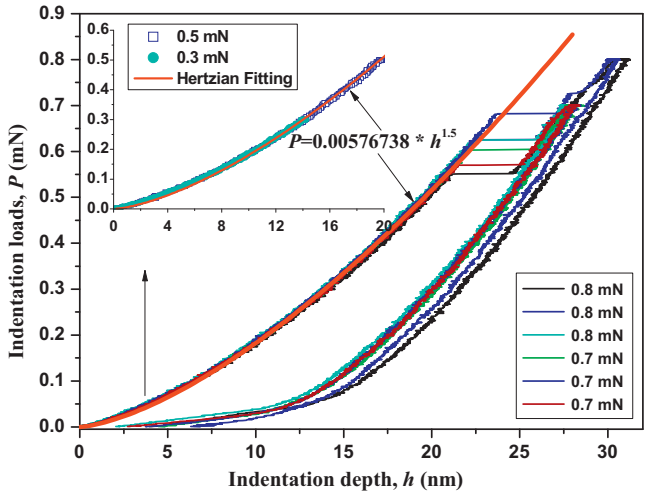

Fig. 7. Typical load–displacement curves of the first pop-in events for the C plane at small size scale. Inset is purely elastic loading and unloading behavior exhibited in the C plane below P_{cr}. The experimental data fit well with the prediction of the Hertzian contact theory before the transition of elastic–plastic deformation.

the anisotropic elasticity formula gives $E_{(0\,0\,0\,1)} = 461.0$ GPa, which is consistent with the experimental results obtained in the range of $h < 60$ nm. Under the anisotropic elastic contact, Swadener et al. obtained that the indentation modulus of the C plane of single-crystal sapphire was about 431 GPa.[13] The measured result by Oliver et al. was 441 ± 4.7 GPa for (0 0 0 1) sapphire during nanoindentation with a Berkovich indenter.[18] Ruppi et al. reported the value of hardness of α-Al_2O_3 with (0 0 0 1) texture was 444 ± 20.7 GPa.[22] Our results in the range of $h > 60$ nm agree well with that form these works.

3.4. Elastic to elastic–plastic transition analysis

The purely elastic and elastic–plastic transitions of the C plane are shown in Fig. 7. To identify the purely elastic behavior of the C plane, more nanoindentation tests with the maximum load of 0.3 and 0.5 mN were performed below P_{cr} (about 0.6 mN), respectively. It is clearly observed that the loading and unloading parts of both load–displacement curves are perfectly superimposed in inset of Fig. 7. It strongly implies that all the samples deform elastically and no residual deformation occurs. It also indicates that the nanoindentation tests have good reproducibility in our tests. Therefore, the deformation can be regarded as perfectly elastic up to a load of 0.5 mN. This is also supported by the SPM imaging after indentation, which shows that the sample surface underneath the indenter is damage-free. In these tests, the maximum nanoindentation depth is 19 nm that is less than 30 nm, so the Berkovich indenter can be approximately considered as spherical.[28] The ideal elastic response of the C plane can be described as $P = (4/3)R^{1/2}E_r h^{3/2}$ by Hertzian contact theory,[23] where P is indentation load, h is indentation depth and R is the radius of spherical indenter tip. A Hertzian equation $P = 0.00576738h^{1.5}$ can be fitted from the indentation data and the relevant curve is shown with red line (see inset), where the units of load P and displacement h are mN and nm, respectively. On the other hand, the coefficient of the equation can be used to verify the calibrated tip radius above. In the purely elastic tests, E_r is about 387 GPa, and R can be deduced as 125 ± 2 nm, which is consistent with the calibration results in Section 3.1 by the standard fused quartz sample and AFM measurements. To further examine the transition from the elastic to elastic–plastic (pop-in) features of the C plane, other nanoindentation tests at the peak load of 0.7 and 0.8 mN were conducted, respectively, as shown in Fig. 7. Both two peak loads are slightly larger than P_{cr} (about 0.6 mN). It is obvious that the typical displacement discontinuities occur during loading. Moreover, the above fitted Hertzian equation is utilized to describe the elastic behavior and elastic–plastic transition. It is interesting to see that the experimental measurement and theoretical prediction fit well before pop-in events.

3.5. Evaluation of slip system and CRSS at slip plane

It is commonly accepted that the initial pop-in event occurs when shear stress acting in the slip direction reaches a critical value, which induces dislocations to move across the slip plane. Generally, the critical shear stress is inversely proportional to the interplanar distance d_{hkl} of the corresponding slip plane because the greater d_{hkl} is, the weaker is the binding force between atoms. It results in the smaller CRSS of a slip system. On the other hand, for hexagonal close packed (hcp) crystal such as sapphire, their elastic–plastic deformations are usually affected by d_{hkl}, the ratio of c/a, loading rate, testing temperature, applied stress and orientation. Compared with the analysis of slip mechanisms of cubic close-packed crystals, the slip and twinning of hcp crystals are more complicated and usually analyzed with the aid of multiple methods, such as transmission electron microscopy,[29,30] high resolution electron microscope and numerical simulations.[9,12] Under the action of an applied stress along the [0 0 0 1] axis, the competition of different slip systems in sapphire crystal would be activated, depending on the value of the critical resolved shear stress (CRSS) and the orientation of slip systems with respect to the external stress. The onset of elastic–plastic transition of the C plane is mainly attributed to slip under such a small indentation load and depth.[4] Based on the reported prevalent slip systems in sapphire, the possibility of activation of the primary slip system in sapphire single crystal was estimated when indenting on the C plane. The similar method applied in the yield point analysis of the cubic crystal was reported by Gerberich et al.[31] In the previous works, the families of slip systems of sapphire crystal were determined by TEM observations[30,32,33] and mainly listed as follows: basal slip $(0\,0\,0\,1)\langle 1\,1\,\bar{2}\,0\rangle$, prism slip $\{1\,1\,\bar{2}\,0\}\langle\bar{1}\,1\,0\,0\rangle$ and pyramidal slips $\{2\,\bar{1}\,\bar{1}\,3\}\langle\bar{1}\,1\,0\,1\rangle$, $\{2\,\bar{1}\,\bar{1}\,3\}\langle 0\,1\,\bar{1}\,0\rangle$, $\{1\,0\,\bar{1}\,1\}\langle\bar{1}\,2\,\bar{1}\,0\rangle$, $\{1\,0\,\bar{1}\,1\}\langle 1\,\bar{1}\,0\,1\rangle$, $\{2\,\bar{1}\,\bar{1}\,2\}\langle 0\,1\,\bar{1}\,0\rangle$ and $\{0\,1\,\bar{1}\,2\}\langle\bar{2}\,0\,2\,1\rangle$. The analysis by the Schmidt law indicates that, among these slip systems, only the Schmidt factors of three pyramidal slips, $\{2\,\bar{1}\,\bar{1}\,3\}\langle\bar{1}\,1\,0\,1\rangle$, $\{1\,0\,\bar{1}\,1\}\langle 1\,\bar{1}\,0\,1\rangle$ and $\{0\,1\,\bar{1}\,2\}\langle\bar{2}\,0\,2\,1\rangle$, are nonzero and equal to 0.407, 0.255 and 0.332, respectively. The inclined angles between the three pyramidal slip planes and indented (0 0 0 1) surface are 61.2°, 72.4° and 57.6°, respectively. Their corresponding $d_{(2\,\bar{1}\,3)}$, $d_{(1\,0\,1)}$ and $d_{(1\,0\,2)}$ are 0.2087,

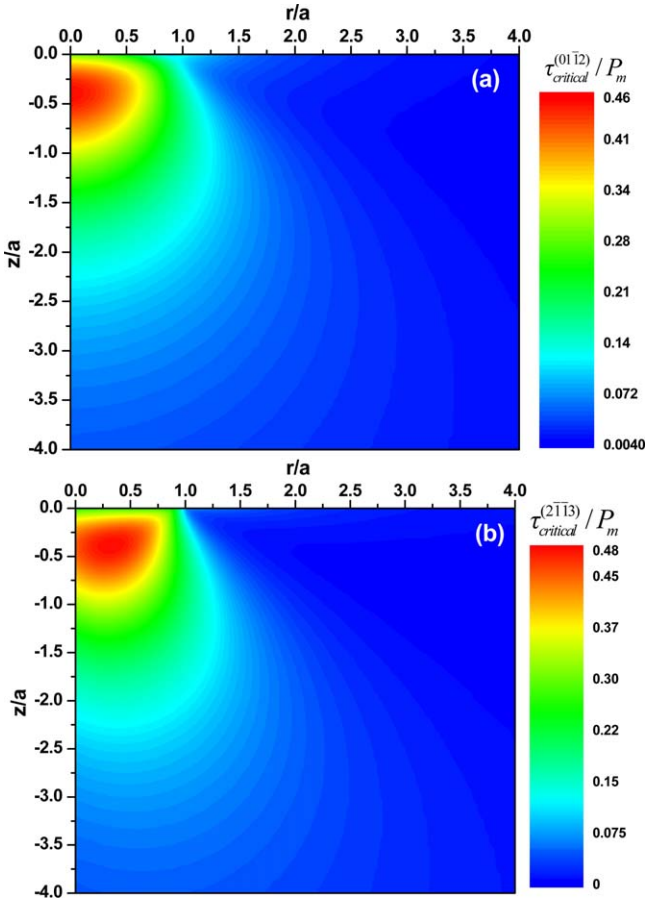

Fig. 8. Contour plot of the CRSS at different slip planes of (a) $(0\,1\,\bar{1}\,2)$ and (b) $(2\,\bar{1}\,\bar{1}\,3)$, where distances r and z are normalized by the contact radius a.

0.3932 and 0.3483 nm, respectively. Therefore, when indenting on the C plane of sapphire crystal, the primary slip system may be due to the competition between pyramidal slips $\{2\,\bar{1}\,\bar{1}\,3\}\langle\bar{1}\,1\,0\,1\rangle$ and $\{0\,1\,\bar{1}\,2\}\langle\bar{2}\,0\,2\,1\rangle$. To further discuss the possible slip deformation, one has to refer to the resolved shear stress of the two families of crystal planes $\{2\,\bar{1}\,\bar{1}\,3\}$ and $\{0\,1\,\bar{1}\,2\}$ during the elastic–plastic transition of the C plane. Considering the hexagonal symmetry of hexagonal sapphire crystals, the Miller-Bravais system (a_1a_2c) is generally transformed into the Cartesian coordinate system $(x_1x_2x_3)$, in which $[2\,\bar{1}\,\bar{1}\,0]$, $[0\,1\,\bar{1}\,0]$ and $[0\,0\,0\,1]$ are a set of Cartesian axes x_1, x_2 and x_3, respectively. In addition, their corresponding stress fields near the indented $(0\,0\,0\,1)$ surface can be estimated by the Hertzian contact theory.[23] After a series of stress alternations in the Cartesian coordinate system, the resolved shear stress distributions of the presumptive two slip planes $(0\,1\,\bar{1}\,2)$ and $(2\,\bar{1}\,\bar{1}\,3)$ were estimated, as shown in Fig. 8(a) and (b), respectively, which were calculated by experimental parameters at small size scale such as, $P_{cr} = 0.613$ mN, $R = 125$ nm, and $E_r = 328.9$ GPa. In Fig. 8, we have the average pressure $P_m = (16PE_r^2/9\pi^3R^2)^{1/3}$ and the contact radius $a = (3PR/4E_r)^{1/3}$. For the slip plane $(0\,1\,\bar{1}\,2)$, the maximum shear stress of 28.8 GPa locates underneath the indenter of coordinates $(r/a = 0, z/a = -0.405)$. For the slip plane $(2\,\bar{1}\,\bar{1}\,3)$, the maximum shear stress of 30.0 GPa locates underneath the indenter of coordinates $(r/a = 0.303,\ z/a = -0.405)$. Previous studies on single crystal and amorphous materials showed that the initial plastic deformation under nanoindentation happens at the shear stress in the absence of dislocations, where G is the shear modulus.[24] For the C plane of sapphire indented along the C axis, the above analysis shows $G = 167$ GPa. Generally, G is about 150–170 GPa in other available experimental data.[29,34] The two maximum critical resolved shear stresses above at the assumed slip planes agree well with the theoretical shear strength, $\tau_{th} \approx G/2\pi = 226.5$ GPa. The results also indicate that the ratio of $\tau^{(0\,1\,\bar{1}\,2)}_{\text{critical}}/P_m$ is approximately equal to $\tau^{(2\,\bar{1}\,\bar{1}\,3)}_{\text{critical}}/P_m$, but $d_{(0\,1\,2)}$ is 1.7 times larger than $d_{(2\,\bar{1}\,3)}$. Therefore, when indenting on the C plane, the primary slip system was estimated as the pyramidal slip $\{0\,1\,\bar{1}\,2\}\langle\bar{2}\,0\,2\,1\rangle$. While the $\{2\,\bar{1}\,\bar{1}\,3\}\langle\bar{1}\,1\,0\,1\rangle$ is considered as a potentially important slip system. With the increase of indentation loads, other slip and subsequent twinning systems may be operated. The movement and interaction of different dislocations would become more complicated.

4. Conclusions

Nanoscale multiple pop-in phenomena of the C plane of sapphire single crystal were clearly observed by nanoindentation contacts at room temperature. The corresponding mechanical properties, stress distribution and deformation mechanism were discussed by the Oliver–Pharr method and Hertzian contact theory, respectively. Main conclusions can be summarized as follows. The critical pop-in loads for the C plane gradually decrease as loading rates increase within the nanoscale indentation depth range. The smaller the loading rate is, the greater the width of pop-in extension becomes. Hardness for the C plane obviously exhibits the indentation size effect. The average H is 46.7 ± 15 GPa at the ISE region and is equal to 27.5 ± 2 GPa at the non-ISE region. The indentation modulus for the C plane decreases with the increase of indentation depth. The steady-state average value of indentation modulus is equal to 420.6 ± 20 GPa when h exceeds to 60 nm. According to the reported prevalent slip systems in sapphire single crystal, the possibility of primary slip systems were analyzed and estimated as the pyramidal slip $\{0\,1\,\bar{1}\,2\}\langle\bar{2}\,0\,2\,1\rangle$ based on the Schmidt law, Hertzian contact theory and crystallography. The contour of critical resolved shear stresses at slip planes were obtained by the Hertzian contact theory.

Acknowledgements

This work was supported by the Research Grant of City University of Hong Kong under Project No. 7002510. The authors thank Mr. K.C. Kian for the help in nanoindentation experiments.

References

1. Heuer AH, Jia CL, Lagerlöf KPD. The core structure of basal dislocations in deformed sapphire (α-Al_2O_3). *Science* 2010;**330**(6008):1227–31.
2. Morikawa J, Orie A, Hashimoto T, Juodkazis S. Thermal and optical properties of the femtosecond-laser-structured and stress-induced birefringent regions in sapphire. *Optics Express* 2010;**18**(8):8300–10.

3. Kudrius T, Slekys G, Juodkazis S. Surface-texturing of sapphire by femtosecond laser pulses for photonic applications. *J Phys D: Appl Phys* 2010;**43**(14):145501.
4. Tymiak NI, Daugela A, Wyrobek TJ, Warren OL. Acoustic emission monitoring of the earliest stages of contact-induced plasticity in sapphire. *Acta Mater* 2004;**52**(3):553–63.
5. Page TF, Oliver WC, Mchargue CJ. The deformation-behavior of ceramic crystals subjected to very low load (nano)indentations. *J Mater Res* 1992;**7**(2):450–73.
6. Pirouz P, Lawlor BF, Geipel T, BildeSorensen JB, Heuer AH, Lagerlöf KPD. On basal slip and basal twinning in sapphire (α-Al_2O_3). 2. A new model of basal twinning. *Acta Mater* 1996;**44**(5):2153–64.
7. Nowak R, Sekino T, Niihara K. Surface deformation of sapphire crystal. *Philos Mag A* 1996;**74**(1):171–94.
8. Nowak R, Sekino T, Maruno S, Niihara K. Deformation of sapphire induced by a spherical indentation on the (10(1)over-bar0) plane. *Appl Phys Lett* 1996;**68**(8):1063–5.
9. Nowak R, Manninen T, Heiskanen K, Sekino T, Hikasa A, Niihara K, et al. Peculiar surface deformation of sapphire: numerical simulation of nanoindentation. *Appl Phys Lett* 2003;**83**(25):5214–6.
10. Tymiak NI, Gerberich WW. Initial stages of contact-induced plasticity in sapphire. I. Surface traces of slip and twinning. *Philos Mag* 2007;**87**(33):5143–68.
11. Tymiak NI, Gerberich WW. Initial stages of contact-induced plasticity in sapphire. II. Mechanisms of plasticity initiation. *Philos Mag* 2007;**87**(33):5169–88.
12. Tymiak N, Chrobak D, Gerberich W, Warren O, Nowak R. Role of competition between slip and twinning in nanoscale deformation of sapphire. *Phys Rev B* 2009;**79**(17):174116.
13. Swadener JG, Pharr GM. Indentation of elastically anisotropic half-spaces by cones and parabolae of revolution. *Philos Mag A* 2001;**81**(2):447–66.
14. Navamathavan R, Park S-J, Hahn J-H, Choi CK. Nanoindentation "pop-in" phenomenon in epitaxial ZnO thin films on sapphire substrates. *Mater Charact* 2008;**59**(4):359–64.
15. Fujikane M, Leszczyski M, Nagao S, Nakayama T, Yamanaka S, Niihara K, et al. Elastic–plastic transition during nanoindentation in bulk GaN crystal. *J Alloys Compd* 2008;**450**(1–2):405–11.
16. Oliver WC, Pharr GM. Measurement of hardness and elastic modulus by instrumented indentation: advances in understanding and refinements to methodology. *J Mater Res* 2004;**19**(1):3–20.
17. Jeong SM, Shum PW, Shen YG, Li KY, Mai YW, Lee HL. Determination of effective nanoindentation range for hard (Ti Al)N thin film. *Jpn J Appl Phys 1* 2006;**45**(8A):6411–6.
18. Oliver WC, Pharr GM. An improved technique for determining hardness and elastic-modulus using load and displacement sensing indentation experiments. *J Mater Res* 1992;**7**(6):1564–83.
19. VanLandingham MR, Juliano TF, Hagon MJ. Measuring tip shape for instrumented indentation using atomic force microscopy. *Meas Sci Technol* 2005;**16**(11):2173–85.
20. Nowak R, Li CL, Swain MV. Comparison of implantation with Ni^{2+} and Au^{2+} ions on the indentation response of sapphire. *Mater Sci Eng A* 1998;**253**(1–2):167–77.
21. Wang Y, Tam PL, Shen YG. Behavior of $Ti_{0.5}Al_{0.5}N$ thin film in nanoscale deformation with different loading rates. *Thin Solid Films* 2008;**516**(21):7641–7.
22. Ruppi S, Larsson A, Flink A. Nanoindentation hardness, texture and microstructure of alpha-Al_2O_3 and kappa-Al_2O_3 coatings. *Thin Solid Films* 2008;**516**(18):5959–66.
23. Fischer-Cripps AC. *Introduction to contact mechanics*. 2nd ed. New York: Springer; 2000.
24. Bei H, Lu ZP, George EP. Theoretical strength and the onset of plasticity in bulk metallic glasses investigated by nanoindentation with a spherical indenter. *Phys Rev Lett* 2004;**93**(12):125504.
25. Albayrak IC, Basu S, Sakulich A, Yeheskel O, Barsoum MW. Elastic and mechanical properties of polycrystalline transparent yttria as determined by indentation techniques. *J Am Ceram Soc* 2010;**93**(7):2028–34.
26. Dey A, Mukhopadhyay AK, Gangadharan S, Sinha MK, Basu D, Bandyopadhyay NR. Nanoindentation study of microplasma sprayed hydroxyapatite coating. *Ceram Int* 2009;**35**(6):2295–304.
27. Yonenaga I, Shima T, Sluiter MHF. Nano-indentation hardness and elastic moduli of bulk single-crystal AlN. *Jpn J Appl Phy 1* 2002;**41**(7A): 4620–1.
28. Bei H, George EP, Hay JL, Pharr GM. Influence of indenter tip geometry on elastic deformation during nanoindentation. *Phys Rev Lett* 2005;**95**(4):045501.
29. Rodriguez MC, Castaing J, Munoz A, Veyssiere P, Rodriguez AD. α-Al2O3 sapphire and rubies deformed by dual basal slip at intermediate temperatures (900–1300 °C). I. Dislocation organization. *Acta Mater* 2009;**57**(10):2873–8.
30. Lloyd SJ, Molina-Aldareguia JM, Clegg WJ. Deformation under nanoindents in sapphire, spinel and magnesia examined using transmission electron microscopy. *Philos Mag A* 2002;**82**(10):1963–9.
31. Gerberich WW, Nelson JC, Lilleodden ET, Anderson P, Wyrobek JT. Indentation induced dislocation nucleation: the initial yield point. *Acta Mater* 1996;**44**(9):3585–98.
32. Barceinas-Sanchez JDO, Rainforth WM. On the role of plastic deformation during the mild wear of alumina. *Acta Mater* 1998;**46**(18):6475–83.
33. Inkson BJ. Dislocations and twinning activated by the abrasion of Al_2O_3. *Acta Mater* 2000;**48**(8):1883–95.
34. Nakamura A, Lagerlöf KPD, Matsunaga K, Tohma J, Yamamoto T, Ikuhara Y. Control of dislocation configuration in sapphire. *Acta Mater* 2005;**53**(2):455–62.